Araştırma Makalesi -Research Article

A Study on the Structural, Morphological and Optical Properties of Cu$_{2-x}$se Thin Films Deposited by Thermal Evaporation

Termal Buharlaştırma ile Üretilen Cu$_{2-x}$Se İnce Filmlerin Yapısal, Morfolojik ve Optik Özellikleri Üzerine Araştırma

Makbule Terlemezoglu[1*]

ABSTRACT

In this work, the influence of post-annealing on the structural, morphological, and optical properties of copper selenide thin films deposited on glass substrate by thermal evaporation was investigated in detail. The post-annealing process at different ambient temperatures in a nitrogen atmosphere was applied to thin films deposited at room temperature. The X-ray diffraction (XRD) patterns showed the presence of cubic Cu$_{2-x}$Se phase, and it was observed that the crystallinity improves with increasing annealing temperature. In addition, it was deduced that the average crystallite size increased with the annealing temperature. Scanning electron microscopy (SEM) and atomic force microscopy (AFM) were employed to investigate the surface morphology of thin films. It was seen that all samples have compact and densely packed surface morphology and grains on the surface become larger. Surface roughness increased from 11nm to 53 nm as the annealing temperature increased. On the other hand, the optical properties of as-deposited and annealed thin films were investigated by utilizing a UV-Visible spectrophotometer. The direct bandgap energies of as-deposited and annealed samples were estimated to be 2.34 eV, 2.31 eV, and 2.29 eV by using the well-known Tauc relation, respectively. The direct bandgap energy of thin films was also calculated using the derivative spectroscopy technique.

Keywords- Thin Film, Characterization, Post-annealing, Semiconductor, Thermal Evaporation

ÖZ

Bu çalışmada, termal buharlaştırma yöntemi ile cam alttaşlar üzerine kaplanmış bakır selenür ince filmlerin yapısal, morfolojik ve optik özelliklerine, üretim sonrası ısıl işlemin etkisi detaylı olarak araştırıldı.Oda sıcaklığında üretilen ince filmlere, azot gazı altında farklı sıcaklıklarda üretim sonrasıısıl işlem uygulandı. X ışını kırınım (XRD) deseni analizi, üretilmiş filmlerin kübik yapıda Cu$_{2-x}$Se fazında olduğunu ve ısıl işlem sıcaklığı arttıkça filmlerin kristalleşme seviyesinin arttığını gösterdi. Ayrıca, artan sıcaklıkla ortalama kristal boyutunun arttığı sonucu elde edildi. Filmlerin yüzey morfolojisini araştırmak için taramalı elektron mikroskobu ve atomik kuvvet mikroskobu kullanıldı. Filmlerin kompakt ve sıkı paketlenmiş yüzey morfolojisine sahip olduğu ve artan ısıl işlem sıcaklığı ile yüzeydeki tanelerin boyutlarının arttığı görüldü.Isıl işlem sıcaklığı arttıkça, yüzey pürüzlülüğü 11 nm'den 53 nm'ye yükseldi. Diğer yandan, üretilen ve ısıl işlem uygulanan ince filmlerin optik özellikleri, ultraviyole- görünür ışık spektrofotometrekullanılarakincelendi. Filmlerin direkt bant aralıkları, iyi bilinen Tauc bağıntısı kullanılarak sırasıyla 2.34eV, 2.31eV ve 2.29 eV olarak bulundu. Ayrıca, ince filmlerin direkt bant aralıkları türev spektroskopi tekniği kullanılarak da hesaplandı.

Anahtar Kelimeler- İnce Film, Karakterizasyon, Üretim Sonrası Isıl İşlem, Yarıiletken, Termal Buharlaştırma

[1*]Sorumlu yazar iletişim: tmakbule@nku.edu.tr (https://orcid.org/0000-0001-7912-0176)
Department of Physics, Tekirdag Namik Kemal University, Tekirdag, Turkey

I. INTRODUCTION

Fabrication and characterization of metal chalcogenide thin films including metal sulfides and metal selenides have gained attention in the last decades due to their superior properties for various applications[1,2]. Particularly, copper selenide thin films have received considerable attention due to their potential in solar cells, gas sensors, supercapacitors, nano switches, medical devices, and photocatalysis applications[3–6]. Copper selenide is a p-type semiconductor having low electrical resistance, and it has suitable bandgap energy and absorption coefficient, as well as earth-abundant and low-cost material [7,8]. Copper selenide can exist in many phases and crystal structures (hexagonal, cubic, tetragonal, orthorhombic, etc.) having different bandgaps, which are stoichiometric ($CuSe$, Cu_2Se, Cu_3Se_2, $CuSe_2$) and non-stoichiometric ($Cu_{2-x}Se$) phases. Among them, non-stoichiometric $Cu_{2-x}Se$ having a face-centered cubic (FCC) structure (space group Fm3m) is often achieved during the synthesizing process[9,10]. $Cu_{2-x}Se$ thin films have a high potential to use in Schottky diodes and absorber layers for solar cells. Besides, it is used as a precursor for copper gallium indium diselenide (CIGS) thin film solar cells and it is frequently encountered as a secondary phase in CZTSe thin film solar cells. Therefore, it is necessary to investigate the physical properties of $Cu_{2-x}Se$ thin films [10–12].

There are many techniques for the growth of copper selenide films which are chemical bath deposition [1], the hydrothermal method [13], electrodeposition [14], atomic layer deposition [3], thermal evaporation [15,16], magnetron sputtering [7], and pulsed laser deposition method [17]. Among these methods, thermal evaporation has some advantages in terms of controllability and suitability for large-scale production.

The present study aims to elucidate the effect of the post-annealing process on the physical properties of the $Cu_{2-x}Se$ thin films. $Cu_{2-x}Se$ thin films were thermally evaporated on glass substrates at room temperature as single-step deposition. The post-annealing process was applied to samples at different temperatures. The structural, morphological, and optical parameters of as-deposited and annealed $Cu_{2-x}Se$ thin films were investigated utilizing several characterization techniques including X-ray diffraction (XRD), Scanning electron microscopy (SEM), energy-dispersive X-ray spectroscopy (EDS), atomic force microscopy (AFM), and transmission/reflection measurements.

II. MATERIAL AND METHODS

To deposit the copper selenide thin films on soda-lime glass substrates (SLG), a thermal evaporation technique was applied. Copper (1) selenide powder having 99.95% purity was used as a deposition source. Before the deposition process, glass substrates were cleaned chemically in the ultrasonic bath. Subsequently, all samples were dried in an N_2 atmosphere at room temperature. Then, samples were mounted on a substrate holder and loaded into the evaporation system. During the deposition, substrates temperature was kept at room temperature and the chamber pressure was kept at $1x10^{-6}$ Torr nearly. The deposition rate was controlled by Inficon XTM/2 thickness monitor and it was in the range of 2-5 Å s^{-1}. The total thickness of films was adjusted to be 700 nm nearly. After the deposition, samples were exposed to post-annealing under a nitrogen atmosphere to determine the effect of heat treatment on the physical properties of deposited thin films. The annealing temperatures were adjusted to be 200°C and 300°C for half an hour as a result of the optimization process since it was observed that annealing temperatures above 300°C were degrading the film adhesion to the glass substrate. The as-deposited sample was labeled as S1 while the annealed samples at 200°C and 300°C were labeled as S2 and S3, respectively.

A horizontal Lindberg furnace was utilized for the post-annealing process. After the fabrication of thin-film, the total thickness of as-deposited and annealed samples was measured by Dektak 6M profile meter within the error limit of 5nm. The morphological investigations and elemental atomic compositions of as-deposited and annealed samples were carried out by using scanning electron microscopy and energy-dispersive X-ray spectroscopy (SEM, Zeiss EVO16 SEM attached to the EDX detector). The phase compositions of the samples were determined by X-ray diffraction measurements (Rigaku Miniflex diffractometer having CuKα radiation source). The surface topography of all samples was further characterized by atomic force microscopy (AFM, Nanomagnetic Instruments) in taping mode. The spectral transmission and reflection of samples were conducted with a UV-Vi-NIR spectrophotometer in the wavelength range of 300-1100 nm (Perkin-Elmer Lambda 45).

III. RESULTS AND DISCUSSION

Figure 1 shows the XRD patterns of all samples. All diffraction peaks of samples were well matched with the standard pattern of cubic $Cu_{2-x}Se$ phase (JCPDS No. 06-0680). According to the standard card for $Cu_{2-x}Se$ phase, diffraction peaks at 2θ°~ 27.1°, 44.8º, 53.1° were labeled as (111), (022) and (113) crystal planes in Figure 1, respectively [9,18].
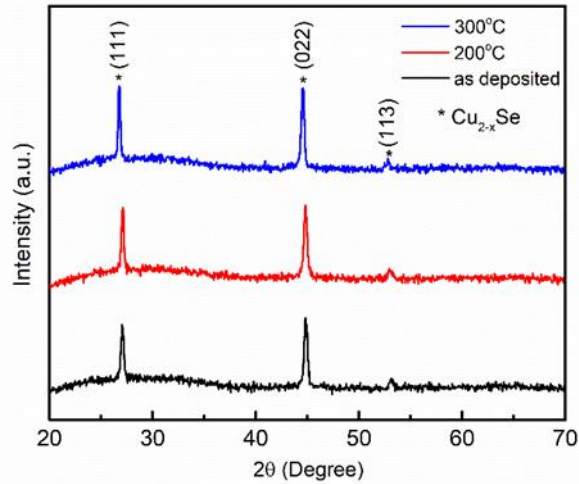
Figure 1. XRD patterns of the S1, S2 and S3 samples

It was observed that there are no characteristic peaks that belong to other phases of copper selenide in the patterns. Higher intensity of diffraction peaks was observed with increasing annealing temperatures, which indicates the improvement in crystallinity. The (022) plane is the most intense peak in the XRD pattern of all samples and this peak was utilized to the estimation of the average crystallite size (D) taking into consideration of Scherrer's relation [19,20]:

$$D = \frac{K\lambda}{\beta \cos \theta} \qquad (1)$$

where λ is the wavelength of X-ray, K is the shape factor, β is the full-width half maximum (FWHM) of diffraction peak in radian, θ is the half of the Bragg diffraction angle. The average crystallite sizes were estimated to be 24 nm, 25 nm, and 27 nm for the S1, S2 and S3 samples, respectively (as shown in Table 1). This indicates the formation of larger grains with increasing post-annealing temperature.

Table 1. Structural parameters of S1, S2, and S3 samples

Samples	Peak Degree (º)	Diffraction Plane	Crystallite size (nm)	Dislocation Density (δ) (m^{-2})	Lattice Strain (LS)
S1	44.8	(022)	24	1.7×10^{15}	0.0037
S2	44.8	(022)	25	1.6×10^{15}	0.0036
S3	44.5	(022)	27	1.3×10^{15}	0.0034

dislocation density (δ) and lattice strain (LS) values were also found to compare the structural parameters of samples by using the following expressions [21],

$$\delta = \frac{1}{D^2} \qquad (2)$$

$$LS = \frac{\beta}{4 \tan \theta} \qquad (3)$$

A decreasing trend was observed in dislocation density and lattice strain with increasing annealing temperatures. It means that the annealing process improves the crystalline level of deposited films. All calculated structural parameters from the XRD measurement were given in Table 1. Table 2 demonstrates the atomic percentages of the S1, S2, and S3 samples obtained by EDS measurements. It is seen that the ratio of the atomic percentages (Cu/Se) of samples confirmed the presence of the $Cu_{2-x}Se$ phase. It was also observed that atomic percentages of Se in S3 decreased, which may be attributed to the re-evaporation of the selenium at high

temperatures. Thus, it can be deduced that post-annealing under argon atmosphere leads to a decrease in selenium content when compared to the atomic composition of as-deposited film.

The top-view SEM images of S1, S2, and S3 samples were presented in Figure 2. The surface of all samples has well-covered, uniform, and dense-packed morphology. It can be seen that annealing temperature affects the surface morphology of thin films directly. While the surface of sample S1 has relatively smooth, that of S2 has a columnar structure. On the other hand, the surface of S3 has some voids which may be due to the re-evaporation of selenium with the increasing annealing temperature. As seen in Table 2, EDX results justify this explanation.

Table 2. Atomic percentages of Cu and Se in the S1, S2 and S3 samples.

Elements	S1	S2	S3
Cu(at%)	63	65	66
Se (at%)	37	35	34

The morphological features of as-deposited and annealed samples were also studied by AFM measurements. Figure 3 shows the three-dimensional AFM images in the size of 5μm x 5μm of S1, S2, and S3 samples. It was seen that surface morphology changes with the annealing process. The grains on the surface increased with the annealing temperatures. The root mean square surface roughness (σ_{RMS}) for S1, S2, and S3 samples were determined as 11nm, 19nm, and 53 nm, respectively. It was obtained that the surface roughness increases as the annealing temperature increases. The increase in surface roughness can provide optical gain in some applications. For this reason, surface roughness is an important parameter for device applications. On the other hand, the optical properties of samples were determined by transmission and reflection measurements in the range of 300-1100 nm. Transmittance (T) and reflectance (R) plots as a function of wavelength of S1, S2, and S3 samples were given in Figure4a. It was observed that there is a sharp increase in transmittance in the vicinity of 550 nm, corresponding to the bandgap of $Cu_{2-x}Se$ phase. The transmittance and reflectance of S2 in the visible region were less than the other samples. This is consistent with the SEM and AFM results since S2 has a columnar structure on the film surface which causes the decrease in reflectance. Using the transmittance and reflectance spectra, the absorption coefficient of samples was calculated employing the following equation [22],

$$T = (1 - R^2)e^{-\alpha t} \tag{4}$$

where α is the absorption coefficient, t is the total thickness of the thin film. The most common method to estimate the optical bandgap (E_g) of a material is the Tauc relation and the expression for direct transition is as follows [19,23],
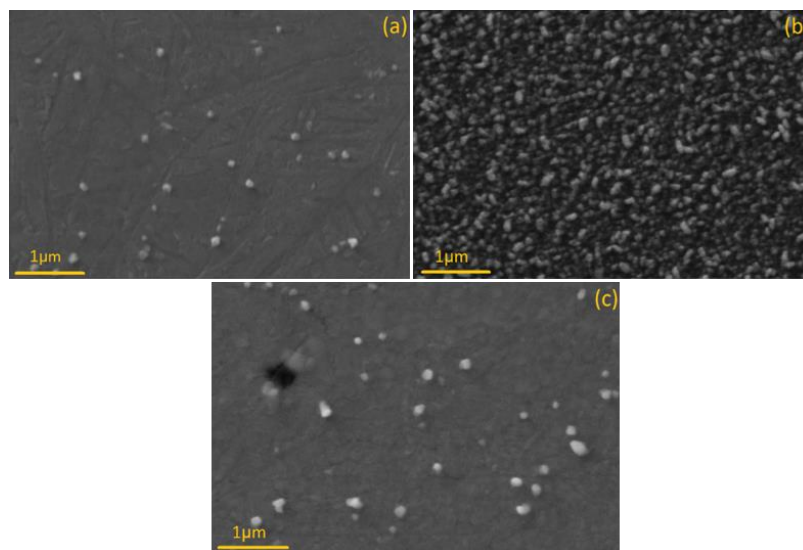
Figure 2. SEM micrographs of (a) S1, (b) S2 and (c) S3 samples
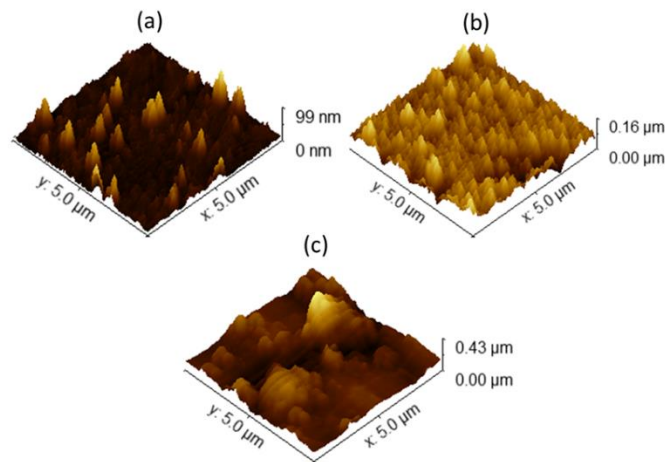
Figure 3. 3D AFM images of S1, S2 and S3 sample from 5μm x 5μm scan area

$$(\alpha h\nu) = A\left(h\nu - E_g\right)^{1/2} \tag{5}$$

In strong absorption region, the plot of $(\alpha h\nu)^2$ vs $(h\nu)$ gives the linear region. The intercept point to the energy axis of the linear part is the bandgap energy. According to Figure 4(b), using the linearity of the strong absorption region, the bandgap energy of S1, S2, and S3 samples were found to be 2.34, 2.31, and 2.29eV, respectively. This is in good agreement with previously reported research [7]. In addition, the derivative spectroscopy technique was employed to expand this work on the estimation of the value of E_g. In this technique, the plot of the first-order derivative of the transmittance with respect to wavelength $\left(\frac{dT}{d\lambda}\right)$ gives a peak, corresponding to the optical bandgap energy [24]. The peak positions were illustrated in the inset of Figure 4 (b). The bandgap energy of S1, S2, and S3 samples were found around to be 2.28, 2.23, and 2.21eV, respectively. There was observed a slight difference in the peak position as the annealing temperature increased, that is, there was a bandgap shift slightly. This can be attributed to several reasons such as improvement in crystallinity, variation in density of impurities, and the Burstein-Moss effect [25-26].
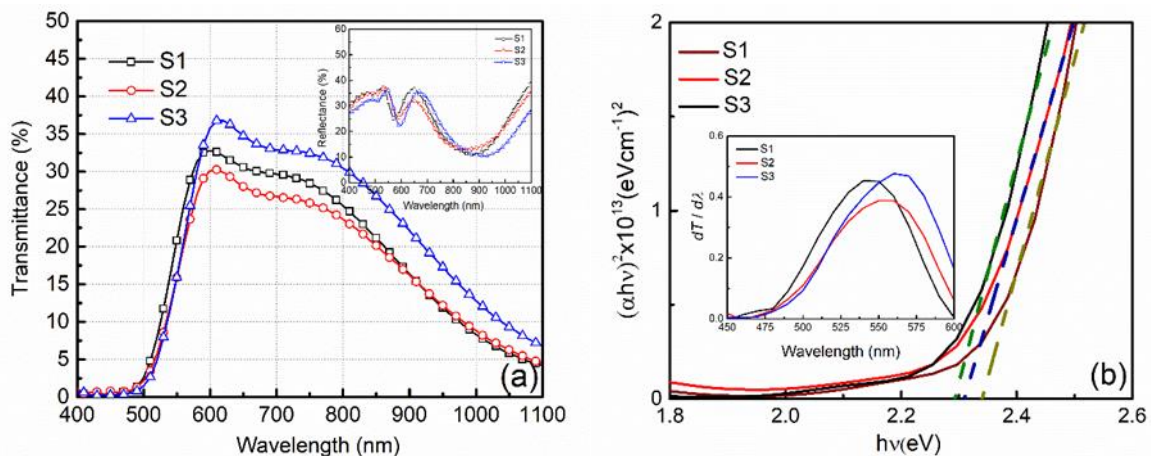
Figure 4. (a) Transmittance spectra (inset shows the reflectance spectra), (b) (αhν)²vs hν plots (inset is the first-order derivative of transmittance spectra) of S1, S2, and S3 samples.

IV. CONCLUSION

In this study, the effect of the post-annealing process on the structural, morphological, and optical properties of Cu$_{2-x}$Se thin films on glass substrates that were deposited by thermal evaporation. The post-annealing processes were carried out at 200ºC and 300ºC for half an hour. The XRD patterns of samples demonstrated preferential orientation along the (022) plane and cubic phase of Cu$_{2-x}$Se. With increasing annealing temperature,

it was observed that the XRD peak related to preferential orientation becomes more intense. According to the results of SEM and AFM measurements, although grains on the surface increased with increasing annealing temperatures, deterioration was observed on the surface of the sample which was annealed at 300ºC. Using the transmission and reflectance spectra of samples, the direct bandgap energies of samples were found to be 2.34, 2.31, and 2.29 eV, respectively. As a result of all measurements, it was observed that the annealing process at 200ºC paves the way for enhancement in all physical properties of $Cu_{2-x}Se$ films while higher annealing temperature leads to deterioration in the surface morphology and related physical features.

ACKNOWLEDGMENT

REFERENCES

[1] Pathan, H., Desai, J., & Lokhande, C. (2002). Modified chemical deposition and physico-chemical properties of copper sulphide (Cu_2S) thin films. *Applied Surface Science*, 202(1), 47–56.

[2] Zhang, Y., Zhou, Q., Zhu, J., Yan, Q., Dou, S. X., & Sun, W. (2017). Nanostructured Metal Chalcogenides for Energy Storage and Electrocatalysis. *Advanced Functional Materials*, 27(35), 1702317.

[3] Lee, K., & Lee, S. (2021). A nanoscale $Cu_{2-x}Se$ ultrathin film deposited via atomic layer deposition and its memristive effects. *Nanotechnology*, 32(24), 245202.

[4] Ambade, S. B., Mane, R. S., Kale, S. S., Sonawane, S. H., Shaikh, A. V., & Han, S. H. (2006). Chemical synthesis of p-type nanocrystalline copper selenide thin films for heterojunction solar cells. *Applied Surface Science*, 253(4), 2123–2126.

[5] Ni, S., Su, Y., Ai, Z., Hu, J., Yang, Z., Kong, E. S. W., & Zhang, Y. (2016). Bandgap tuning and photocatalytic activities of $CuSe_{1-x}S_x$ nanoflakes. *Ceramics International*, 42(1), 211–219.

[6] Vinod, T. P., Jin, X., & Kim, J. (2011). Hexagonal nanoplatelets of CuSe synthesized through facile solution phase reaction. *Materials Research Bulletin*, 46(3), 340–344.

[7] Li, Y. Z., Gao, X. D., Yang, C., & Huang, F. Q. (2010). The effects of sputtering power on optical and electrical properties of copper selenide thin films deposited by magnetron sputtering. *Journal of Alloys and Compounds*, 505(2), 623–627.

[8] Li, Y. D., Fan, P., Zheng, Z. H., Luo, J. T., Liang, G. X., & Guo, S. Z. (2016). The influence of heat treatments on the thermoelectric properties of copper selenide thin films prepared by ion beam sputtering deposition. *Journal of Alloys and Compounds*, 658, 880–884.

[9] Quiao, L.N., Wang, H. C., Shen, Y., Lin., Y.H., & Nan, C. W. (2017). Enhanced Photocatalytic Performance under Visible and Near-Infrared Irradiation of $Cu_{1.8}Se/Cu_3Se_2$ Composite via a Phase Junction. Nanomaterials (Basel, Switzerland), 7(1).

[10] Gu, Y., Su, Y., Chen, D., Geng, H., Li, Z., Zhang, L., & Zhang, Y. (2014). Hydrothermal synthesis of hexagonal CuSe nanoflakes with excellent sunlight-driven photocatalytic activity. *Cryst Eng Comm*, 16(39), 9185–9190.

[11] Bayraklı, Ö., Terlemezoglu, M., Güllü, H. H., & Parlak, M. (2017). Investigation of precursor sequence and post-annealing effects on the properties of $Cu_2SnZnSe_4$ thin films deposited by the elemental thermal evaporation. *Materials Research Express*, 4(8), 086411.

[12] Tanaka, T., Sueishi, T., Saito, K., Guo, Q., Nishio, M., Yu, K. M., & Walukiewicz, W. (2012). Existence and removal of Cu_2Se second phase in coevaporated $Cu_2ZnSnSe_4$ thin films. *Journal of Applied Physics*, 111(5), 053522.

[13] Zhang, G., Zhu, L., & Ba, N. (2016). Hydrothermal synthesis of hexagonal $Cu_{2-x}Se$ microplates and optical properties. *Materials Engineering and Environmental Science,* 158–164.

[14] Lippkow, D., & Strehblow, H. H. (1998). Structural investigations of thin films of copper–selenide electrodeposited at elevated temperatures. *Electrochimica Acta*, 43(14–15), 2131–2140.

[15] Okimura, H., Matsumae, T., & Makabe, R. (1980). Electrical properties of $Cu_{2-x}S$ ethin films and their application for solar cells. *Thin Solid Films*, 71(1), 53–59.

[16] Peranantham, P., Jeyachandran, Y. L., Viswanathan, C., Praveena, N. N., Chitra, P. C., Mangalaraj, D., & Narayandass, S. K. (2007). The effect of annealing on vacuum-evaporated copper selenide and indium telluride thin films. *Materials Characterization*, 58(8–9), 756–764.

[17] Xue, M.Z., Zhou, Y.N., Zhang, B., Yu, L., Zhang, H., & Fu, Z.-W. (2006). Fabrication and Electrochemical Characterization of Copper Selenide Thin Films by Pulsed Laser Deposition. *Journal of The Electrochemical*

Society, 153(12), A2262.

[18] Astam, A., Akaltun, Y., & Yildirim, M. (2016). Conversion of SILAR deposited Cu_3Se_2 thin films to $Cu_{2-x}Se$ by annealing. *MaterialsLetters*, 166, 9–11.

[19] Surucu, O., Isik, M., Terlemezoglu, M., Gasanly, N. M., & Parlak, M. (2021). Structural and temperature-tuned bandgap characteristics of thermally evaporated β-In2S3 thin films. *Journal of Materials Science: Materials in Electronics* 2021 32:12, 32(12), 15851–15856.

[20] Terlemezoglu, M., Bayrakli Sürücü, O., Colakoğlu, T., Abak, M. K., Güllü, H. H., Ercelebi, C., & Parlak, M. (2019). Construction of self-assembled vertical nanoflakes on CZTSSe thin films. *Materials Research Express*. 6(2),026421.

[21] Erturk, K., Isik, M., Terlemezoglu, M., & Gasanly, N. M. (2021). Optical and structural characteristics of electrodeposited $Cd_{1-x}Zn_xS$ nanostructured thin films. Optical Materials, 114, 110966.

[22] Terlemezoglu, M., Bayraklı Sürücü, Ö., Dogru, C., Güllü, H. H., Ciftpinar, E. H., Erçelebi, Ç., & Parlak, M. (2019). CZTSSe thin films fabricated by single step deposition for superstrate solar cell applications. *Journal of Materials Science: Materials in Electronics*, 30, 11301–11306.

[23] Surucu, O., Isik, M., Gasanly, N. M., Terlemezoglu, M., & Parlak, M. (2020). Temperature-tuned band gap properties of MoS_2 thin films. *Materials Letters*, 275, 128080.

[24] Caglar, Y., Caglar, M., Ilican, S., & Ates, A. (2009). Morphological, optical and electrical properties of CdZnO films prepared by sol–gel method. Journal of Physics D: Applied Physics, 42(6), 065421.

[25] Akin, N., Kinaci, B., Ozen, Y., & Ozcelik, S. (2017). Influence of RF power on the opto-electrical and structural properties of gallium-doped zinc oxide thin films. Journal of Materials Science: Materials in Electronics, 28(10), 7376–7384.

[26] López-Suárez, A., Acosta, D., Magaña, C., & Hernández, F. (2020). Optical, structural and electrical properties of ZnO thin films doped with Mn. Journal of Materials Science: Materials in Electronics, 31(10), 7389–7397.